symmetry

MDPI

Article

Coupling Hadron-Hadron Thresholds within a Chiral Quark Model Approach

Pablo G. Ortega [1,†] and David R. Entem [2,*,†]

[1] Department of Fundamental Physics and IUFFyM, U. Salamanca, E-37008 Salamanca, Spain; pgortega@usal.es
[2] Grupo de Física Nuclear and IUFFyM, U. Salamanca, E-37008 Salamanca, Spain
* Correspondence: entem@usal.es
† These authors contributed equally to this work.

Abstract: Heavy hadron spectroscopy was well understood within the naive quark model until the end of the past century. However, in 2003, the $X(3872)$ was discovered, with puzzling properties difficult to understand in the simple naive quark model picture. This state made clear that excited states of heavy mesons should be coupled to two-meson states in order to understand not only the masses but, in some cases, unexpected decay properties. In this work, we will give an overview of a way in which the naive quark model can be complemented with the coupling to two hadron thresholds. This program has been already applied to the heavy meson spectrum with the chiral quark model, and we show some examples where thresholds are of special relevance.

Keywords: naive quark model; unquenched quark model; hadron resonances; virtual states; coupled channels

check for updates

Citation: Ortega, P.G.; Entem, D.R. Coupling Hadron-Hadron Thresholds within a Chiral Quark Model Approach. *Symmetry* **2021**, *13*, 279. https://doi.org/10.3390/sym13020279

Academic Editor: Vladimir V. Vechernin
Received: 18 December 2020
Accepted: 2 February 2021
Published: 6 February 2021

Publisher's Note: MDPI stays neutral with regard to jurisdictional claims in published maps and institutional affiliations.

Copyright: © 2021 by the authors. Licensee MDPI, Basel, Switzerland. This article is an open access article distributed under the terms and conditions of the Creative Commons Attribution (CC BY) license (https://creativecommons.org/licenses/by/4.0/).

1. Introduction

Heavy hadron spectroscopy started in November 1974, when Brookhaven National Laboratory announced the discovery of a new particle called J [1] and, at the same time, the Stanford Linear Accelerator reported the existence of another new particle, called ψ [2]. Very soon, both particles were seen as the same state, which we know now as the J/ψ state of the charmonium spectrum. This state was understood as a $q\bar{q}$ bound state in the naive quark model, and its discovery was the confirmation of the existence of the charm quark that was predicted by the GIM mechanism [3] a few years before.

Afterwards, heavy meson spectroscopy developed very fast during the following years. The $\Upsilon(1S)$, the first state with bottom quarks discovered, was found at Fermilab [4] in 1977. Already in 1980, there were 11 new mesons included in the Particle Data Group (PDG) table [5] on these energy ranges, but that rate decreased to only 15 new states added during the period 1980 to 2003 [6]. However, during these last 17 years, 35 new states have been added [7], considering only unflavored mesons.

In the case of the baryon spectra, the first evidence of charmed baryons came six months after the discovery of the J/ψ, in 1975 [8], but, in 1980, only the Λ_c and Σ_c baryons were included in the heavy baryon spectrum of the PDG [5]. In 2003, only 14 states were identified [6], while again, during the last 17 years, 33 new states have been included [7].

This impressive development of the heavy hadron spectrum has been possible thanks in part to the so called B-factories, like Belle and BaBar, which are electron–positron colliders tuned to the center of mass energy of the $\Upsilon(4S)$ that decays into two B mesons. Other facilities like BESIII, with a lower energy electron–positron collider, have contributed. Many impressive results have also been obtained and are underway at LHC by the LHCb, CMS, and ATLAS Collaborations. The next generation Super$B$-factory Belle II is running from 2018, and it is expected to make many important contributions to heavy hadron physics.

From a theoretical point of view, the description of the hadron spectroscopy has mostly relied on potential models since the discovery of the J/ψ meson. Regarding heavy quarkonium spectroscopy, potential models have been very successful at describing the charmonium and bottomonium spectra (see, e.g., [9–17]). It is worth mentioning that new theoretical approaches directly derived from QCD, such as Effective Field Theories (EFTs) like non-relativistic QCD (NRQCD) [18–20] or lattice gauge theories [21–23] have been recently employed to study hadron spectroscopy. However, due to their complexity, many features of the hadron spectroscopy are more easily addressed with potential model approaches. Already in 1978, the Cornell model [24] was developed to understand heavy meson spectroscopy. This model is a non-relativistic approach for heavy quarks with interactions that are governed by $SU(3)$ color gauge symmetry, with the flavor only broken by the quark masses. The main pieces of the model are a Coulomb-like interaction, inspired by the one-gluon exchange, and a linear term, which describes the confining effect. It also took into account two important features that one expects from QCD, Heavy Flavor Symmetry (HFS) and Heavy Quark Spin Symmetry (HQSS), considering terms that are flavor and spin independent. The naive quark model from Cornell was fitted to the only 11 states that were known in 1978 and gave a quite good description of the charmonium and bottomonium spectrum at that time [25]. Not only that, the predictions were in quite good agreement with the experiments up to 2003, giving a prediction for 15 new states in the correct energy range. The Cornell potential has been related with the QCD static potential by Sumino [26] and more recently with NRQCD up to N^3LO [27].

For the baryon spectra, also very soon, in 1979, quark models developed for the light sector were applied in the heavy quark sector [28]. In addition, Stanley and Robsen [29] extended the Cornell model to study heavy baryons. Many new states were predicted, but it took a long time to be seen on experiments.

Until 2003, the simple naive quark model picture was in quite good agreement with experiments. However, already in the original Cornell model [24], the coupling with two-meson thresholds was considered for excited states, although it was found to be of no relevance for the states considered at that time. The key event in 2003 for heavy hadron spectroscopy was the discovery of the $X(3872)$ by the Belle Collaboration [30]. It was very soon confirmed by the CDF [31], D0 [32], and BaBar [33] Collaborations. It has some intriguing properties that are difficult to understand in the naive quark model picture but easily explained when coupled channel effects are included.

Nevertheless, one of the clearest indications that coupled-channel effects have to be considered are the famous pentaquarks measured by LHCb [34,35]. These states are unflavored baryons in the region of 4.5 GeV which rules out a three-light quark baryon interpretation. The only possible explanation is a pentaquark with three light quarks and a $c\bar{c}$ pair. Whether these states are compact pentaquarks or baryon-meson molecules is a matter of intense debate, although the closeness of these states to different meson–baryon thresholds is seen as a clear indication of the second possibility.

In this work, we will make a brief overview of coupled-channel effects in the framework of the quark model, in the same spirit as the original Cornell model. Thus, we will use naive quark-model states coupled to two-hadron channels, also built from naive quark-model states. The coupling between these two different sectors will be obtained using the microscopic $^3P_0$ creation model. The paper is organized as follows: In Section 2, we will give a brief introduction to the naive chiral quark model and how to calculate the spectrum in this picture. In Section 3, we will give the basis of the $^3P_0$ model and how to evaluate the transition amplitude. Section 4 will be devoted to present the formalism to couple one and two-hadron states. In Section 5, we will show a few examples in the meson spectrum where such effects are relevant and show some results in the quark model picture. We will end with some conclusions.

2. The Naive Chiral Quark Model

The quark model we use is a constituent quark model based on spontaneous chiral symmetry breaking [36]. It was first applied to the light-quark sector [37] and then extended to the heavy sector [38].

The main ingredients of the model are the following. The spontaneous chiral symmetry breaking generates two important effects in the light-quark sector. On one side, the light quarks acquire a dynamical mass that, at zero momentum, is of the order of 330 MeV for the u and d quarks, and 550 MeV for the s quark. This dynamical effect has been seen on the lattice [39], and it is the idea introduced phenomenologically in the constituent quark model. On the other side, it introduces the interaction of light quarks through the exchange of pseudo-Goldstone bosons. Another important non-perturbative effect is confinement, seen as the fact that hadrons are only seen in color singlets. We include it phenomenologically using a linear screened confinement interaction. This effect has also been observed in lattice QCD, where, in quenched QCD, a linear rising of the energy of two static sources with increasing distance is clearly seen [40] and, in unquenched QCD, this string is broken [41] when there is enough energy to produce a quark–antiquark pair. Finally, we introduce QCD perturbative effects through the one-gluon exchange interaction [42]. The model has been reviewed in many works, and all of the details can be found in Refs. [43,44].

Once the model interaction is settled, in order to obtain the hadron wave functions, one has to solve a non-relativistic bound equation for the two-body problem, in the case of mesons, as quark–antiquark pairs or the three body problem, for baryons, as three-quark states. There are many different approaches to solve these systems. The problem can be solved in coordinate space, in momentum space or using the Rayleigh–Ritz variational principle using a certain basis function. Sometimes, the potential involved poses special problems for some technique. For example, the use of a Coulomb-like potential makes the diagonal part of the potential in momentum space logarithmically divergent, which introduces a numerical problem. On the other hand, if we use a non-local interaction in coordinate space, the Schrödinger equation ends up being an integro-differential equation, which is also numerically more demanding. Another important fact is whether coupled channels are considered or not. Momentum space calculations or variational calculations are very easily extended to such a case, while coordinate space calculations are not straightforwardly extended.

Nonetheless, the method that can be usually used in any case is the variational method. This method is specially interesting for our purposes since we will be able to calculate transition amplitudes based on the $^3P_0$ model with matrix elements of the basis functions used.

The main problem of the method is to find the appropriate basis functions. There are many different options for many different systems. However, the Gaussian Expansion Method (GEM) has been shown to be a very good approach in almost any case. The method was firstly proposed by Kamimura [45] and has been applied to many few body problems [46,47].

In the case of the two-body problem, the employed basis functions are a set of Gaussians multiplied by a solid-spherical harmonic in the relative coordinate, to take into account the correct behavior of the wave function at the origin

$$\varphi_{nlm}(\vec{r}) = N_{nl} r^l e^{-\nu_n r^2} Y_{lm}(\hat{r}) \quad (1)$$

$$N_{nl} = \left(\frac{2^{l+2} (2\nu_n)^{l+3/2}}{\sqrt{\pi}(2l+1)!!} \right)^{1/2}. \quad (2)$$

The basis function is generated by taking several values for the Gaussian parameter ν_n. In the GEM, these parameters are taken in geometrical progression as

$$\nu_n = \frac{1}{r_n^2} \tag{3}$$

$$r_n = r_{\min} a^{n-1} \tag{4}$$

$$a = \left(\frac{r_{\max}}{r_{\min}}\right)^{\frac{1}{N-1}} \tag{5}$$

where $r_{\min}$ and $r_{\max}$ are the minimum and maximum radius and N the number of Gaussians. $r_{\min}$ and $r_{\max}$ should be chosen such that the range of the wave functions is well represented. For excited states, usually the range increases, so states with a higher range than $r_{\max}$ will not be correctly represented. $r_{\min}$ should be below the range of the potential. Numerically, it is important that the parameter a is not too close to 1 so that the problem does not become singular, so N can not be increased arbitrarily for fixed values of $r_{\min}$ and $r_{\max}$. Then, one can use the expansion

$$\varphi(\vec{r}) = \sum_{nl} c_{nl} \varphi_{nlm}(\vec{r}) \tag{6}$$

and ends up with the generalized eigenvalue problem

$$\sum_{nl} (H_{n'l',nl} - E N_{n'l',nl}) c_{nl} = 0 \tag{7}$$

with

$$H_{n'l',nl} = \langle \varphi_{n'l'm} | H | \varphi_{nlm} \rangle \tag{8}$$

$$N_{n'l',nl} = \langle \varphi_{n'l'm} | \varphi_{nlm} \rangle . \tag{9}$$

In the case of the naive quark model, one has to include the spin–flavor–color degrees of freedom so the total wave function is

$$\varphi(\vec{r}) = \sum_{nl} c_{nl} \left[\varphi_{nl}(\vec{r}) \chi_S \right]_J \chi_F \xi_c \tag{10}$$

where χ_S is the spin wave function, χ_F is the flavor wave function, and ξ_c is the color singlet quark–antiquark wave function and where the orbital angular momentum l is coupled with the spin S to total angular momentum J.

As a matter of fact, the GEM is more interesting when we have more than two interacting particles. Usually, one chooses a set of coordinates that includes the center of mass, so one solves for the relative motion of the interacting particles. Then, one builds the most general wave function with the desired total quantum numbers. This is usually done considering an expansion in angular momentum of the different coordinates and one assumes that, for short-range interactions, only the lowest partial waves will be needed. To have a feeling of what is needed, typical accurate three-body Fadeev calculations of Triton binding energy need up to 38 of such partial waves. The GEM approaches the problem in a different way; it also considers the lowest partial waves, although not only in one set of possible Jacobi coordinates, but in different sets. This has been shown to have a much faster convergence than the previous approach, which numerically is less demanding because radial wave functions in a lower number of partial waves are needed. The drawback is that now different partial waves are not orthogonal, so they cannot be considered separately.

In the case of the three-body problem, there are three different sets of Jacobi coordinates given by

$$\vec{R}_{cm} = \frac{m_1\vec{u}_1 + m_2\vec{u}_2 + m_3\vec{u}_3}{M_T} \tag{11}$$

$$\vec{r}_i = \vec{u}_j - \vec{u}_k \tag{12}$$

$$\vec{R}_i = \vec{u}_i - \frac{m_j\vec{u}_j + m_k\vec{u}_k}{m_j + m_k} \tag{13}$$

where $\vec{u}_i$ is the position vector of particle i, and (ijk) is one of the three even permutations of (123). The orbital wave function is taken as

$$\varphi = \sum_{i=1}^{3} \sum_{n_i l_i N_i L_i} c_{n_i l_i N_i L_i} \left[\varphi_{n_i l_i}(\vec{r}_i)\varphi_{N_i L_i}(\vec{R}_i)\right]_{L_T} \tag{14}$$

where $(-1)^{l_i+L_i}$ gives the parity, and L_T is the total orbital angular momentum. If there are identical particles, some relations between different modes i may be needed. These relations can be easily obtained from the action of the permutation operator

$$P_{ij}\left[\varphi_{n_i l_i}(\vec{r}_i)\varphi_{N_i L_i}(\vec{R}_i)\right]_{L_T} = (-1)^{l_i}\left[\varphi_{n_i l_i}(\vec{r}_j)\varphi_{N_i L_i}(\vec{R}_j)\right]_{L_T} \tag{15}$$

$$P_{ij}\left[\varphi_{n_j l_j}(\vec{r}_j)\varphi_{N_j L_j}(\vec{R}_j)\right]_{L_T} = (-1)^{l_j}\left[\varphi_{n_j l_j}(\vec{r}_i)\varphi_{N_j L_j}(\vec{R}_i)\right]_{L_T} \tag{16}$$

$$P_{ij}\left[\varphi_{n_k l_k}(\vec{r}_k)\varphi_{N_k L_k}(\vec{R}_k)\right]_{L_T} = (-1)^{l_k}\left[\varphi_{n_k l_k}(\vec{r}_k)\varphi_{N_k L_k}(\vec{R}_k)\right]_{L_T}. \tag{17}$$

If we consider, for example, the Helium atom, with particle 1 being the nuclei and particles 2 and 3 the electrons, then we can consider two different wave functions with definite symmetry against the P_{23} operator

$$\varphi = \sum_{n_1 l_1 N_1 L_1} c_{n_1 l_1 N_1 L_1}\left[\varphi_{n_1 l_1}(\vec{r}_1)\varphi_{N_1 L_1}(\vec{R}_1)\right]_{L_T} \tag{18}$$

$$\varphi = \sum_{n_{23} l_{23} N_{23} L_{23}} c_{n_{23} l_{23} N_{23} L_{23}}\left\{\left[\varphi_{n_{23} l_{23}}(\vec{r}_2)\varphi_{N_{23} L_{23}}(\vec{R}_2)\right]_{L_T} \pm \left[\varphi_{n_{23} l_{23}}(\vec{r}_3)\varphi_{N_{23} L_{23}}(\vec{R}_3)\right]_{L_T}\right\} \tag{19}$$

where the symmetry to the exchange of the electrons is $(-1)^{l_1}$ in the first case and $\pm(-1)^{l_{23}}$ for the second case. In principle, one could only work with one basis including all possible angular momentums but numerically is more efficient to use both with the lower angular momentum. Then, the spin wave functions of the electrons have to be considered to solve the wave functions for parahelium ($S = 0$) and orthohelium ($S = 1$). In Tables 1 and 2, we show the ground state and first excited states for parahelium and orthohelium, respectively, compared to experimental data from the NIST database. Here, we only include Coulomb interactions so we should expect deviations of the order of $\alpha^2 \sim 10^{-4}$. As we can see, even with a long-range interaction such as the Coulomb one, the GEM works very well.

Table 1. First levels of parahelium ($S = 0$) with orbital angular momentum $L \leq 2$. The experimental data are taken from NIST, Ref. [48]—results with the GEM method from this work. All energies are in eV.

	Term	J	**NIST**	**GEM**
$1s^2$	^1S	0	0.00000000	0.00
$1s2s$	^1S	0	20.6157751334	20.61
$1s2p$	^1P	1	21.2180230218	21.21
$1s3s$	^1S	0	22.920317682	22.91
$1s3d$	^1D	2	23.07407511941	23.07
$1s3p$	^1P	1	23.0870188528	23.08
$1s4s$	^1S	0	23.6735709133	23.67
$1s4d$	^1D	2	23.73633535786	23.73
$1s4p$	^1P	1	23.7420703918	23.74
$1s5s$	^1S	0	24.0112153129	24.00
$1s5d$	^1D	2	24.042803734930	24.04
$1s5p$	^1P	1	24.0458007297	24.04
$1s6s$	^1S	0	24.1911605982	24.18
$1s6d$	^1D	2	24.209250116893	24.20

If the three particles are identical, then the wave function to be used is

$$\varphi \quad = \quad \sum_{nlNL} c_{nlNL} \sum_{i=1}^{3} \left[\varphi_{nl}(\vec{r}_i) \varphi_{NL}(\vec{R}_i) \right]_{L_T} . \tag{20}$$

As explained above, we have to include the spin–flavor–color wave function for baryons in a quark model where, again, the spin is coupled with the total orbital angular momentum L_T to give a total angular momentum J, and the color wave function corresponds to the color singlet.

The GEM is again very accurate and, in Table 3, we give the result of ground state heavy baryons in the Bhaduri [49] model, calculated with the GEM and compared with a Fadeev calculation by B. Silvestre-Brac [50]. The GEM calculation only includes wave functions with $l_i = L_i = 0$. In addition, the matter radius square and the charge radius square defined by

$$\langle R_m^2 \rangle \quad = \quad \langle \Psi | \sum_{i=1}^{3} \frac{m_i}{M} (\vec{u}_i - \vec{R}_{cm})^2 | \Psi \rangle \tag{21}$$

$$\langle R_c^2 \rangle \quad = \quad \langle \Psi | \sum_{i=1}^{3} e_i (\vec{u}_i - \vec{R}_{cm})^2 | \Psi \rangle \tag{22}$$

are given. From the results, one expects to have a good approximation to the solution of the three-body problem using the GEM.

Table 2. First levels of orthohelium ($S = 1$) with orbital angular momentum $L \leq 2$. The experimental data are taken from NIST, Ref. [48]—results with the GEM method from this work. All energies are in eV.

	Term	J	**NIST**	**GEM**
$1s2s$	$3S$	1	19.81961484203	19.82
$1s2p$	$3P$	2	20.96408720675	20.98
		1	20.96409668230	
		0	20.96421916817	
$1s3s$	$3S$	1	22.718466742	22.71
$1s3p$	$3P$	2	23.0070734673	23.01
		1	23.0070761918	
		0	23.0071097475	
$1s3d$	$3D$	3	23.07365102990	23.07
		2	23.07365134140	
		1	23.07365682165	
$1s4s$	$3S$	1	23.593959036	23.59
$1s4p$	$3P$	2	23.7078915511	23.71
		1	23.7078926664	
		0	23.7079063452	
$1s4d$	$3D$	3	23.73609051247	23.73
		2	23.73609066143	
		1	23.73609295768	
$1s5s$	$3S$	1	23.9719717413	23.97
$1s5p$	$3P$	2	24.0282253870	24.02
		1	24.0282259477	
		0	24.0282328220	
$1s5d$	$3D$	3	24.042662564819	24.04
		2	24.042662644310	
		1	24.042663817021	
$1s6s$	$3S$	1	24.1689985463	24.16
$1s6p$	$3P$	2	24.2008157776	24.20
		1	24.2008160981	
		0	24.2008200312	
$1s6d$	$3D$	3	24.209163433335	24.22
		2	24.209163480258	
		1	24.209164158016	

However, not all the states are below the lowest open threshold. If we again consider the Helium atom, the first ionization occurs at an energy of 24.587389011 eV [51], when the continuum of a ground state of a He^+ atom and a free electron starts. As the GEM takes boundary conditions for bound states, one can still find these bound states as shown in Table 4, although it is more difficult. These states can decay into a $He^+ + e^-$ so they are resonances and can be seen on scattering processes. In the case of hadrons, there is a similar situation; however, quarks can not abandon a hadron, and a quark–antiquark pair is produced to generate two hadron states.

Table 3. results for the Bhaduri potential obtained with a Fadeev calculation (FD) [50] and the GEM method (this work). Masses are given in MeV, while matter radius square R_m^2 and charge radius square R_c^2 are in fm^2.

State	M(FD)	M(GEM)	R_m^2(FD)	R_m^2(GEM)	R_c^2(FD)	R_c^2(GEM)
$\Lambda_c^+(cud)$	2300	2298.5	0.097	0.0984	0.117	0.1180
$\Sigma_c^0(cud)$	2473	2475.0	0.111	0.1116	−0.224	−0.2247
$\Sigma_c^+(cud)$					0.134	0.1347
$\Sigma_c^{++}(cud)$					0.494	0.4941
$\Lambda_b(bud)$	5653	5649.6	0.043	0.0435	0.115	0.1169
$\Sigma_b^-(bud)$	5858	5859.8	0.051	0.0509	−0.280	−0.2804
$\Sigma_b^0(bud)$					0.138	0.1383
$\Sigma_b^+(bud)$					0.555	0.5571
$\Xi_c^0(nsc)$	2490	2490.9	0.097	0.0978	−0.145	−0.1463
$\Xi_c^+(nsc)$					0.160	0.1617
$\Omega_c^0(css)$	2700	2701.0	0.100	0.0999	−0.111	−0.1111
$\Xi_b^-(nsb)$	5826	5824.8	0.045	0.0459	−0.193	−0.1951
$\Xi_b^0(nsb)$					0.151	0.1517
$\Omega_b^-(bss)$	6046	6046.7	0.050	0.0505	−0.164	−0.1642
$\Xi_{cc}^+(ncc)$	3631	3632.2	0.076	0.0766	−0.034	−0.0330
$\Xi_{cc}^{++}(ncc)$					0.285	0.2852
$\Xi_{bb}^-(nbb)$	10,197	10,197.4	0.031	0.0309	−0.128	−0.1279
$\Xi_{bb}^0(nbb)$					0.215	0.2140
$\Omega_{cc}^+(scc)$	3739	3738.7	0.073	0.0739	0.008	0.0091
$\Omega_{cb}^+(scb)$	7023	7024.2	0.043	0.0430	−0.023	−0.0232
$\Omega_{bb}^-(sbb)$	10,271	10,271.3	0.030	0.0304	−0.083	−0.0829
$\Omega_{ccc}^{++}(ccc)$	4806	4807.2	0.062	0.0619	0.124	0.1239
$\Omega_{ccb}^+(ccb)$	8032	8030.9	0.038	0.0378	0.089	0.0891
$\Omega_{cbb}^0(cbb)$	11,220	11,218.6	0.026	0.0264	0.032	0.0318
$\Omega_{bbb}^-(bbb)$	14,370	14,371.8	0.019	0.0192	−0.019	−0.0192

Table 4. Levels of orthohelium ($S = 1$) above the first open threshold. The experimental data are taken from NIST, Refs. [52,53]—results with the GEM method from this work. All energies are in eV.

	Term	NIST	GEM
$2s2p$	^3P	58.311 [52]	58.31
$2p^2$	^3P	59.67378 [53]	59.66
$2p3p$	^3D	63.120 [52]	
$2p3d$	^3D	63.78658 [52]	
$2p3d$	^3P	64.0719 [52]	

3. The $^3P_0$ Model

The quark–pair creation model or $^3P_0$ model is a microscopic model that allows for coupling channels with different number of quarks (Figure 1). The name comes from the fact that a quark–antiquark pair is created with quantum numbers of the vacuum. It was first proposed by Micu [54] and, afterwards, Le Yaouanc et al. applied it to the strong decays of mesons [55] and baryons [56]. These authors also evaluated strong decay partial widths of the three charmonium states $\psi(3770)$, $\psi(4040)$, and $\psi(4415)$ within the same model [57,58].

The $^3P_0$ model is usually formulated in terms of the Hamiltonian operator

$$H_I = \sqrt{3}\, g_s \int d^3x\, \bar{\psi}(\vec{x})\psi(\vec{x}) \tag{23}$$

where the only parameter of the model is g_s. The factor $\sqrt{3}$ is usually not included, but, in our case, cancels the color factor in the meson sector, so g_s has the usual definition.

It can be also formulated in terms of a transition operator given by

$$T = -\sqrt{3}\sum_{\mu,\nu}\int d^3p_\mu d^3p_\nu \delta^{(3)}(\vec{p}_\mu + \vec{p}_\nu)\frac{g_s}{2m_\mu}\sqrt{2^5\pi}\times\left[\mathcal{Y}_1\left(\frac{\vec{p}_\mu - \vec{p}_\nu}{2}\right)\otimes\left(\frac{1}{2}\frac{1}{2}\right)1\right]_0 a^\dagger_\mu(\vec{p}_\mu)b^\dagger_\nu(\vec{p}_\nu) \tag{24}$$

where μ (ν) are the spin, flavor, and color quantum numbers of the created quark (antiquark). The spin of the quark and antiquark is coupled to one. The $\mathcal{Y}_{lm}(\vec{p}\,) = p^l Y_{lm}(\hat{p})$ is the solid harmonic defined as a function of the spherical harmonic.

It is common to give the transition operator in terms of the strength of the quark–antiquark pair creation from the vacuum γ as in Ref. [59]. The relation is given as

$$\gamma = g_s/2m \tag{25}$$

m being the mass of the pair created, which is usually a light pair.

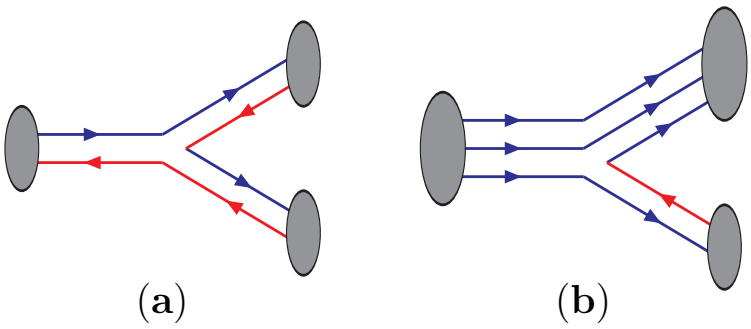


Figure 1. Diagrams of the $^3P_0$ model that contributes to the decay of a meson into two mesons (**a**) and a baryon into a baryon and a meson (**b**).

We consider a process where an initial hadron A decays into two final hadrons B and C. When we work in the center of mass system of the initial hadron, we have $\vec{P}_A = \vec{P}_{cm} = 0$, with $\vec{P}_A$ the momentum of the initial hadron and $\vec{P}_{cm}$ the total momentum of the final hadrons. Then, the matrix element of the transition operator is written as

$$\langle BC|T|A\rangle = \delta^{(3)}(\vec{P}_{cm})\mathcal{M}_{A\to BC}\,. \tag{26}$$

The matrix element is taken between hadron states written in terms of quark degrees of freedom in second quantization. Meson and baryon states are written as

$$|M\rangle = \int \phi_M(1,2)b^\dagger_1 d^\dagger_2|0\rangle d^3p_1 d^3p_2 \tag{27}$$

$$|B\rangle = \mathcal{N}_B\int \Psi_B(1,2,3)b^\dagger_1 b^\dagger_2 b^\dagger_3|0\rangle d^3p_1 d^3p_2 d^3p_3 \tag{28}$$

where $b^\dagger$ is a quark creation operator and $d^\dagger$ an antiquark creation operator, $\mathcal{N}_B$ is a factor in terms of the number of identical quarks in the baryon, and with the normalization convention for the wave functions,

$$\sum\int |\phi_M(1,2)|^2 d^3p_1 d^3p_2 = 1 \tag{29}$$

$$\sum\int |\Psi_B(1,2,3)|^2 d^3p_1 d^3p_2 d^3p_3 = 1 \tag{30}$$

where the sum is for discrete degrees of freedom. With these states, two hadron states with correct quantum numbers are constructed.

With the transition amplitude, the widths for strong decays can be evaluated

$$\Gamma_{A\to BC} = 2\pi \frac{E_B(k_0)E_C(k_0)}{m_A k_0} |\mathcal{M}_{A\to BC}(k_0)|^2 \tag{31}$$

with k_0 the relative momentum of the two final hadrons.

The transition amplitude is basically given in terms of the wave function of the naive quark model considered. There are many factors that are given in terms of the quark model symmetries, but also an important form factor is given in terms of the overlap of the initial and final hadron wave functions with the transition operators. The orbital part of the matrix element can be difficult to compute, and this is the reason why the use of the GEM to solve the internal wave function of mesons and baryons is of special interest. The linearity of the operator allows that, using the expansion of the wave function in the GEM basis,

$$|A\rangle = \sum_k c_k |A_k\rangle \tag{32}$$

$$|B\rangle = \sum_i c_i |B_i\rangle \tag{33}$$

$$|C\rangle = \sum_j c_j |C_j\rangle \tag{34}$$

where $|A_k\rangle$, $|B_k\rangle$, and $|C_k\rangle$ are the different GEM components for the hadrons and the c's the coefficients for the solution of the GEM, one can evaluate the matrix element in terms of matrix elements in the GEM basis as

$$\langle BC|T|A\rangle = \sum_{ijk} c_i^* c_j^* c_k \langle B_i C_j|T|A_j\rangle \tag{35}$$

where the matrix elements in the GEM basis $\langle B_i C_j|T|A_j\rangle$ are evaluated analytically.

Once the naive quark model is fixed, the only unknown to determine the transition amplitude is the $^3P_0$ strength parameter γ. In the case of meson decays, a scale-dependent parameter was considered in Ref. [60] as

$$\gamma(\mu) = \frac{\gamma_0}{\log(\frac{\mu}{\mu_0})} \tag{36}$$

with $\gamma_0 = 0.821 \pm 0.02$ and $\mu_0 = (49.84 \pm 2.58)$ MeV. The scale is taken as the reduced mass of the quarks on the initial meson. The parameters were fixed to the strong width of a few open-charm, charmonium, and bottomonium states and, then, applied to many different states on these sectors. However, it is interesting to notice that this scale dependence was able to predict the strong decay widths of open-bottom mesons correctly without including this sector on the fit.

4. The Unquenched Quark Model

The unquenched quark model [61] or unitarized quark models [62] include the effects of two-hadron thresholds in one hadron state through hadron loops. They are usually implemented with approximate wave functions, and the interaction between the two-hadrons in the loops is not considered. Here, we present how these effects can be incorporated in an easy way.

In the previous section, we showed how one and two-hadron states are connected and give rise to the strong decay widths. However, the same transition amplitude has as a consequence: the one-hadron and two-hadron states connected gets mixed. As the origin is

the strong force, this mixing can be sizable. For this reason, in some cases, it is important to consider the effect and, for this purpose, we consider the physical state as

$$|\Psi\rangle = \sum_{\alpha} c_{\alpha}|\psi_{\alpha}\rangle + \sum_{\beta}\chi_{\beta}(P)|\psi_{H1}\psi_{H2}\beta\rangle \tag{37}$$

where $|\psi_{\alpha}\rangle$ are naive quark model one-hadron states with α quantum numbers and $|\psi_{H1}\psi_{H2}\beta\rangle$ are two-hadron state H_1H_2 with β quantum numbers and relative momentum P. We define now the transition amplitude

$$\langle\psi_{H1}\psi_{H2}\beta|T|\psi_{\alpha}\rangle = P\,\delta^{(3)}(\vec{P}_{cm})h_{\beta\alpha}(P)\,. \tag{38}$$

If we impose the Schrödinger equation

$$H|\Psi\rangle = E|\Psi\rangle \tag{39}$$

and solve for the one-hadron amplitudes, we find

$$c_{\alpha} = \frac{1}{E - M_{\alpha}}\sum_{\beta}\int h_{\alpha\beta}(P)\chi_{\beta}(P)P^2dP \tag{40}$$

where $\chi_{\beta}(P)$ is given by the equation in the two-hadron sector

$$\sum_{\beta}\int\left(H^{H_1H_2}_{\beta'\beta}(P',P) + V^{\rm eff}_{\beta'\beta}(P',P)\right)\chi_{\beta}(P)P^2dP = E\chi_{\beta'}(P')\,. \tag{41}$$

Here, $H^{H_1H_2}_{\beta'\beta}(P',P)$ is the Hamiltonian generated by the kinetic energy of all the quarks and interaction between pairs of quarks that depend on the relative momentum of the hadrons, since the other degrees of freedom are fixed by the hadron states. There is also a part of the interaction which is generated by the coupling with one-hadron states and is given by

$$V^{\rm eff}_{\beta'\beta}(P',P) = \sum_{\alpha}\frac{h_{\beta'\alpha}(P')h_{\alpha\beta}(P)}{E - M_{\alpha}}\,. \tag{42}$$

It is interesting to notice that this effective potential has special relevance at an energy close to the threshold of a two meson channel β, $E \sim E^{\rm thr}_{\beta}$, where one expects the molecules to appear. Furthermore, one should expect attraction for $E \sim E^{\rm thr}_{\beta} < M_{\alpha}$ since $V^{eff}_{\beta\beta}(P,P) < 0$ and there is repulsion in the other case, it being more intense when the bare state is closer to the threshold $M_{\alpha} \sim E^{\rm thr}_{\beta}$. Thus, states above threshold will help to bind a molecule while states below threshold will help to unbind it. This analysis helps to know when a dynamically generated state can appear.

This formalism is suitable for bound states. However, in order to solve the scattering or consider resonances, it is convenient to work with the equivalent Lippmann–Schwinger equation written as

$$T^{\beta'\beta}(E;P',P) = V_T^{\beta'\beta}(P',P) + \sum_{\beta''}\int dP''P''^2V_T^{\beta'\beta''}(P',P'')\frac{1}{E - E_{\beta''}(P'')}T^{\beta''\beta}(E;P'',P) \tag{43}$$

with

$$V_T^{\beta'\beta}(P',P) = V^{\beta'\beta}(P',P) + V^{\beta'\beta}_{\rm eff}(P',P) \tag{44}$$

$$H^{H_1H_2}_{\beta'\beta}(P',P) = \delta_{\beta'\beta}\frac{\delta(P'-P)}{P^2}\frac{P^2}{2\mu_{\beta}} + V^{\beta'\beta}(P',P)\,. \tag{45}$$

The solution to this equation is given in Ref. [63]

$$T^{\beta'\beta}(E;P',P) = T_V^{\beta'\beta}(E;P',P) + \sum_{\alpha,\alpha'} \phi^{\beta'\alpha'}(E;P')\Delta^{-1}_{\alpha'\alpha}(E)\bar{\phi}^{\alpha\beta}(E;P)\,. \tag{46}$$

The first term on the right-hand side is the non-resonant contribution given by the solution of the equation

$$T_V^{\beta'\beta}(E;P',P) = V^{\beta'\beta}(P',P) + \sum_{\beta''}\int dP'' P''^2 V^{\beta'\beta''}(P',P'')\frac{1}{E-E_{\beta''}(P'')}T_V^{\beta''\beta}(E;P'',P)\,. \tag{47}$$

The resonant part include the dressed vertex functions

$$\phi^{\alpha\beta'}(E;P) = h_{\alpha\beta'}(P) - \sum_{\beta}\int \frac{T_V^{\beta'\beta}(E;P,q)h_{\alpha\beta}(q)}{q^2/2\mu_\beta - E}\,q^2\,dq, \tag{48}$$

$$\bar{\phi}^{\alpha\beta}(E;P) = h_{\alpha\beta}(P) - \sum_{\beta'}\int \frac{h_{\alpha\beta'}(q)T_V^{\beta'\beta}(E;q,P)}{q^2/2\mu_{\beta'} - E}\,q^2\,dq \tag{49}$$

and the dressed two hadron propagator defined as the inverse of

$$\Delta^{\alpha'\alpha}(E) = \Big\{(E-M_\alpha)\delta^{\alpha'\alpha} + \mathcal{G}^{\alpha'\alpha}(E)\Big\}, \tag{50}$$

$$\mathcal{G}^{\alpha'\alpha}(E) = \sum_{\beta}\int dq q^2 \frac{\phi^{\alpha\beta}(q,E)h_{\beta\alpha'}(q)}{q^2/2\mu_\beta - E}\,. \tag{51}$$

The dressed propagator has singularities at the energies of the resonance states so, to find these energies, we solve the equation

$$\Big|\Delta^{\alpha'\alpha}(\bar{E})\Big| = \Big|(\bar{E}-M_\alpha)\delta^{\alpha'\alpha} + \mathcal{G}^{\alpha'\alpha}(\bar{E})\Big| = 0\,. \tag{52}$$

Once the resonance energies $\bar{E}$ are known, we find one-hadron amplitudes by solving

$$\Big\{M_\alpha\delta^{\alpha\alpha'} - \mathcal{G}^{\alpha'\alpha}(\bar{E})\Big\}c_{\alpha'}(\bar{E}) = \bar{E}\,c_\alpha(\bar{E}) \tag{53}$$

and the two-hadron wave function is given by

$$\chi_{\beta'}(P') = -2\mu_{\beta'}\sum_\alpha \frac{\phi_{\beta'\alpha}(E;P')c_\alpha}{P'^2 - k^2_{\beta'}} \tag{54}$$

with $k^2_{\beta'} = 2\mu_{\beta'}(E - E^{\rm thr}_{\beta'})$. Notice that the normalization of the wave-function requires

$$\sum_\alpha |c_\alpha|^2 + \sum_\beta \langle\chi_\beta|\chi_\beta\rangle = 1\,. \tag{55}$$

The solution with naive quark model states $|\psi_\alpha\rangle$ is only exact if all the state α are included. However, including only those states close to the energy range under consideration has been shown to be a good approximation. In Ref. [64], the unquenched quark model for charmonium mesons was considered but solving not only for the relative two-hadron wave function, but for the wave function of the ψ_α meson as a $c\bar{c}$ meson, getting very similar results to the present approximation.

5. Coupled Channel Effects

As mentioned before, since 2003, it has been clear that the naive quark model is not enough to understand the heavy hadron spectra. In some cases, such as the pentaquarks, the energy scale of its mass makes it unavoidable to include higher Fock components.

However, as we will see, in other cases, threshold effects can easily explain properties that are very difficult to understand in the naive quark model. In this section, we give a few examples of such cases and we will summarize results obtained using the model previously introduced.

5.1. Isospin Breaking Effects

The $X(3872)$ was discovered in the $J/\psi\pi\pi$ invariant mass distribution of the $B^+ \to K^+\pi^+\pi^- J/\psi$ decay. The two-pions in this decay came from a ρ^0 meson [65], which is an isospin 1 final state. The ratio of the decay into three pions was also measured, and the three-pions came from the decay of an ω meson [66], which is an isospin 0 channel. The ratio between these two decay modes was found to be

$$\frac{\mathcal{B}(X(3872) \to \pi^+\pi^-\pi^0 J/\psi)}{\mathcal{B}(X(3872) \to \pi^+\pi^- J/\psi)} = 1.0 \pm 0.4(\text{stat}) \pm 0.3(\text{syst})\,. \tag{56}$$

Thus, this state can decay into final states with two different values of isospin, which implies that either isospin is violated in the decay process or the isospin of the $X(3872)$ is not well defined.

The $X(3872)$ is now included in the PDG as the $\chi_{c1}(3872)$. Quark models usually predict this state at higher energies, although the deviation can be explained if one considers that this theoretical state is close and above the $D\bar{D}^*$ threshold. One important question is whether the $X(3872)$ is the state expected in this energy region by quark models, or if it is an additional state dynamically generated in the $D\bar{D}^*$ channel. In any case, the crucial property of this state is that its mass is very close to the $D^0\bar{D}^{*0}$ with a binding energy given by

$$B \equiv m_{D^{*0}} + m_{\bar{D}^0} - m_{X(3872)} = 1.1^{+0.6+0.1}_{-0.4-0.3}\ \text{MeV} \tag{57}$$

$$= (0.00 \pm 0.18)\ \text{MeV} \tag{58}$$

$$= (0.07 \pm 0.12)\ \text{MeV} \tag{59}$$

where the first number is from Ref. [67], the second from Ref. [68], and the third is from Ref. [69].

Since the mass is so close to the $D\bar{D}^*$ threshold, one would expect a molecule or a mixing with some charmonium state. Considering the large isospin breaking, the most promising source is the mass splitting between charge and neutral states of D and D^* mesons, finding

$$m_{D^{*+}} + m_{D^-} - m_{D^{*0}} - m_{\bar{D}^0} = 8.2 \pm 0.1\ \text{MeV} \gg B \tag{60}$$

to be a larger scale than the binding energy, which suggests a big effect. Notice that the masses by themselves do not suggest it, since the breaking is only of 0.13% and 0.08% for the D and D^* mesons, respectively. This effect was introduced by Swanson [70] in a coupled channel calculation in which an isospin 1 channel $J/\psi\rho$ was introduced. The important point to notice is that the binding energy for the charged channel is around 8 MeV, so the size of this component is around 1.5 fm, while, for the neutral, the small binding energy B makes the size of the order of 4 fm or bigger. This effect generates a big isospin breaking on the wave function out of the interaction region. This assertion generated some confusion since the isospin breaking effect is small in the interaction region. The isospin breaking was further analyzed in Ref. [71] in the framework of an Effective Field Theory, where the coupling of the states to the different final channels could be evaluated. The couplings obtained for $D\bar{D}^*$ states were $g = 2982$ MeV and $g = 3005$ MeV for charged and neutral channels, respectively, showing an isospin breaking of less than 1%. In fact, although the ratio given in Equation (56) suggests a big isospin breaking, this is only due to the big phase space effects that enhances the isospin 1 channel against the isospin 0 [71]. Excluding phase space effects, the decay in the ρ channel is only around

3.2% of the ω channel decay. This was clarified in Ref. [72] relating the couplings with the probability of the wave function in the interacting region.

The microscopic calculation at the quark level was performed in Ref. [73] in the framework of the chiral quark model previously described. Within the model, the naive quark model $\chi_{c1}(2P)$ state has a mass of 3947 MeV, which is far above the $X(3872)$. Coupling with $D\bar{D}^*$ states makes the naive quark model masses change slightly. However, the important effect is that a new state appears in the $D\bar{D}^*$ threshold with properties in overall good agreement with those of the $X(3872)$. This is in contrast to other unquenched quark models [74] where the $X(3872)$ is not an additional state but just a corrected naive quark model state by two meson loops.

The ratio of Equation (56) was analyzed in Ref. [75], finding a value close to the experimental result. The big isospin breaking on the wave function is represented in Figure 2. For exact isospin symmetry, the $D\bar{D}^*$ charged and neutral components should have the same probabilities, while we see that, close to the $D\bar{D}^*$ neutral threshold, this component dominates.

This effect, seen on the $X(3872)$ state, may appear in any hadron–hadron molecule close to the threshold. Of particular interest are the famous pentaquark states [34,35], which are close to the $\Sigma_c\bar{D}$, $\Sigma_c^*\bar{D}$, and $\Sigma_c\bar{D}^*$ thresholds. This is the reason why it is widely accepted that the nature of these states is more likely to be a hadron–hadron molecule than a compact pentaquark state. Being close to the threshold, isospin breaking effects were studied [76], and these effects could be magnified in the $P_c(4457)$ [77]. For this state, the binding energy is $2.5^{+1.8}_{-4.2}$ MeV for the charged channel with lower threshold and $6.9^{+1.8}_{-4.1}$ MeV for the higher threshold. Analogously to the decays into $J/\psi\rho$ and $J/\psi\omega$, the pentaquark could decay into an isospin $3/2$ channel $J/\psi\Delta^+$ or an isospin $1/2$ channel $J/\psi p$. Within an EFT framework, the ratio

$$R_{\Delta^+/p} = \frac{|\mathcal{B}(P_c(4457)^+ \to J/\psi\Delta^+)|}{|\mathcal{B}(P_c(4457)^+ \to J/\psi p)|}$$

was evaluated and showed to be up to 30%. The measurement of this isospin violating decay of the pentaquark could be the best indication of its molecular nature.

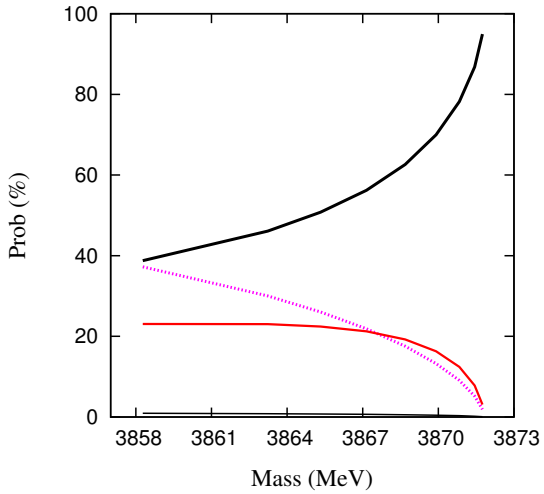


Figure 2. Probabilities of different components in the physical $X(3872)$ state obtained in the unquenched chiral quark model as a function of the mass. The mass is varied using the $^3P_0$ strength parameter. Lines are $D\bar{D}^*$, charged neutral in black and charged channel in red, $\chi_{c1}(2P)$ in dashed magenta and $\chi_{c1}(1P)$ in thin black.

5.2. HQSS and HFS Breaking

Heavy Quark Spin Symmetry (HQSS) and Heavy Flavor Symmetry (HFS) are good approximate symmetries of QCD, so one would expect them to be realized in the heavy hadron spectrum.

If we look into the heavy-light sector, under exact HQSS, the D and D^* mesons should have the same mass. Despite it not exactly being realized, the ratio $\frac{M_{D^*}-M_D}{M_{D^*}+M_D} \sim 3.6\%$ shows that the breaking is, indeed, small. In the hidden charm sector, we have $\frac{M_{J/\psi}-M_{\eta_c}}{M_{J/\psi}+M_{\eta_c}} \sim 1.8\%$ and $\frac{M_{\chi_{c2}(1P)}-M_{\chi_{c0}(1P)}}{M_{\chi_{c2}(1P)}+M_{\chi_{c0}(1P)}} \sim 2.0\%$, so even smaller breaking. HFS implies that interactions do not depend on the heavy quark mass, so, when we find a state in the charm sector, there must exist an analog in the bottom sector.

If we consider the $X(3872)$ to be a $D\bar{D}^*$ molecule, HQSS [78–80] leads to unavoidable predictions. The interaction between $D\bar{D}^*(1^{++})$ and $D^*\bar{D}^*(2^{++})$ channels is the same, so, if the $X(3872)$ is a $D\bar{D}^*(1^{++})$ molecule, it implies that there should be a bound state with very similar binding energy in the $D^*\bar{D}^*(2^{++})$, which was dubbed $X(4012)$. In addition, HFS requires the interaction between charmed mesons to be the same as for bottom mesons [81], so the same molecules observed in the hidden-charm sector should appear in the hidden-bottom sector.

HQSS is usually fulfilled by heavy quark models, since the heavy quark mass only appears in fine structure terms that are suppressed as $1/m_Q$ corrections. Within HQSS, one finds for S partial-waves [82]

$$\frac{2}{\sqrt{3}}\langle D^*\bar{D}^*(0^{++})|H|D\bar{D}(0^{++})\rangle = \langle D\bar{D}(0^{++})|H|D\bar{D}(0^{++})\rangle - \langle D^*\bar{D}^*(0^{++})|H|D^*\bar{D}^*(0^{++})\rangle \quad (61)$$

$$\langle D\bar{D}^*(1^{++})|H|D\bar{D}^*(1^{++})\rangle = \langle D^*\bar{D}^*(2^{++})|H|D^*\bar{D}^*(2^{++})\rangle, \quad (62)$$

$$\langle D\bar{D}^*(1^{++})|H|D\bar{D}^*(1^{++})\rangle = \frac{3}{2}\left[\langle D\bar{D}(0^{++})|H|D\bar{D}(0^{++})\rangle - \frac{1}{3}\langle D^*\bar{D}^*(0^{++})|H|D^*\bar{D}^*(0^{++})\rangle\right] \quad (63)$$

$$2\langle D\bar{D}^*(1^{+-})|H|D\bar{D}^*(1^{+-})\rangle = \langle D\bar{D}(0^{++})|H|D\bar{D}(0^{++})\rangle + \langle D^*\bar{D}^*(0^{++})|H|D^*\bar{D}^*(0^{++})\rangle \quad (64)$$

where H represents the interacting Hamiltonian. In the chiral quark model of previous sections, the results for diagonal matrix elements are shown in Figures 3 and 4, showing that HQSS is approximately fulfilled. Additionally, comparing the matrix elements of the interactions in the charmed and bottom sectors, we can see that HFS is also fulfilled.

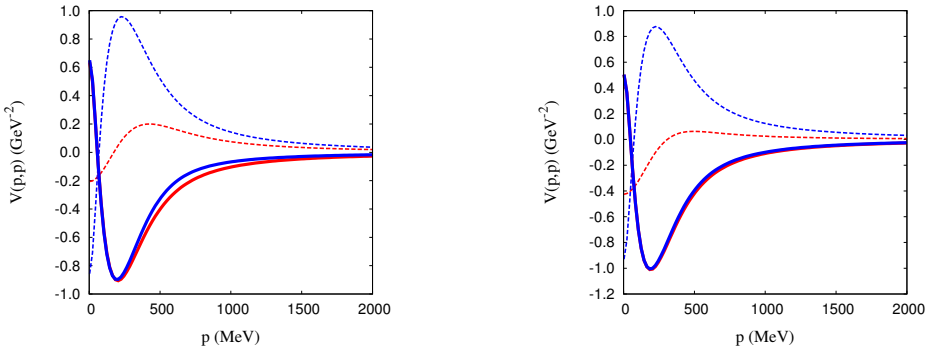


Figure 3. Diagonal matrix elements of the two meson interaction in momentum space for the $D^{(*)}\bar{D}^{(*)}$ sector (left panel) and $B^{(*)}\bar{B}^{(*)}$ sector (right panel). For the left panel, the dashed blue line gives the $D^*\bar{D}^*(0^{++})$ matrix element, the dashed red line the $D\bar{D}(0^{++})$, the solid blue line the right-hand side of Equation (61), and the solid red line left-hand side of the same equation. For the right panel, it is the same but for $B^{(*)}\bar{B}^{(*)}$ channels.

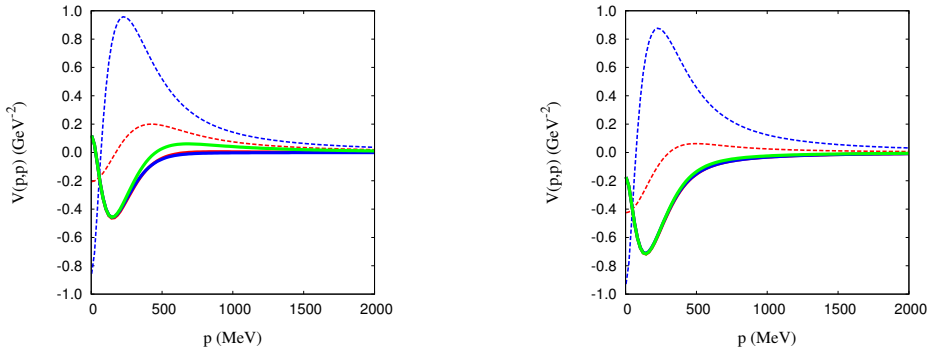


Figure 4. Diagonal matrix elements of the two meson interaction in momentum space for the $D^{(*)}\bar{D}^{(*)}$ sector (left panel) and $B^{(*)}\bar{B}^{(*)}$ sector (right panel). For the left panel, the dashed blue line gives the $D^*\bar{D}^*(0^{++})$ matrix element, the dashed red line the $D\bar{D}(0^{++})$, the solid blue line the right-hand side of Equation (62), the solid red line the left-hand side of the same equation, and the solid green line the right-hand side of Equation (63). At exact HQSS, the three solid lines should be equal. For the right panel, it is the same but for $B^{(*)}\bar{B}^{(*)}$ channels.

Nevertheless, open thresholds appear in energy regions where we can also find naive quark model states, so one-hadron and two-hadron states can be mixed as shown in the previous sections. This effect can have important consequences for states that are mainly dynamically generated molecules. Let's see an example and consider the P-wave charmonium states. Considering the allowed spins, using the spectroscopic notation $^{2S+1}L_J$, we may have the states $^1P_1$ ($J^{PC} = 1^{+-}$), $^3P_0$ (0^{++}), $^3P_1$ (1^{++}) and $^3P_2$ (2^{++}) coupled to $^3F_2$. Under HQSS, all these states are degenerated (within a small deviation due to the breaking). The largest mass splitting is given by the difference of the ground states $M_{\chi_{c2}(1P)} - M_{\chi_{c0}(1P)} \sim 141$ MeV, the splitting for excited states being smaller in the naive quark model picture. The $\chi_{cJ}(2P)$ and $h_c(2P)$ states are in the region of the $D^{(*)}\bar{D}^{(*)}$ thresholds; however, the threshold difference $M_{D^*\bar{D}^*} - M_{D\bar{D}} \sim 282$ MeV is larger. Taking only S-wave two-meson states, only $D\bar{D}$ and $D^*\bar{D}^*$ can have 0^{++} quantum numbers, while only $D\bar{D}^*$ can have 1^{++} and $D^*\bar{D}^*$ can have 2^{++}. This means that the relevant threshold in each channel will have a different relative position with respect to naive quark model states. This is shown in Figure 5, where we can see that, for the 1^{++} channel, the naive quark model state is above the $D\bar{D}^*$ threshold, giving additional attraction, while, in the 2^{++} channel, the P-wave state is below the threshold, giving repulsion (The state above $D^*\bar{D}^*$ threshold is an F state.). This explains why the 1^{++} channel has an additional state, while the 2^{++} does not, which is against HQSS expectations. A systematic study of this effect was performed at the hadron level in Ref. [83], and a more elaborate study at the quark level was performed in Ref. [84].

In bottomonium, we have a different situation. In the 1^{++} channel, the naive quark model state generates repulsion and no additional state appears, while, in the 2^{++} channel, there is attraction from the state above threshold and repulsion from the state below, and the final result is that an additional state appears. This result is, again, against HFS expectations [82]. A more elaborate calculation including more thresholds is underway (Figure 6).

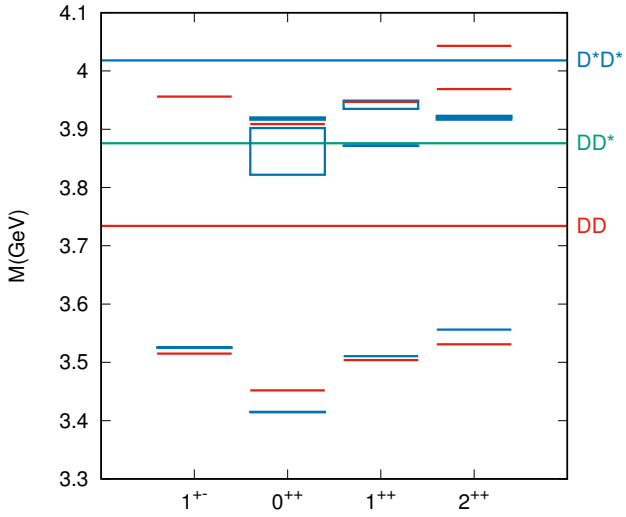


Figure 5. Charmonium spectrum in the energy region of $1P$ and $2P$ states. Blue boxes show the states in the Particle Data Group [7]. The $X(3915)$ has been included in the 0^{++} and in the 2^{++} channels since the J quantum number is not known. The quantum numbers of the $X(3940)$ are also not known, but it has been included in the 1^{++} channel since it has been seen in $D\bar{D}^*$ but not in DD. The states in red are naive $Q\bar{Q}$ states predicted by the model.

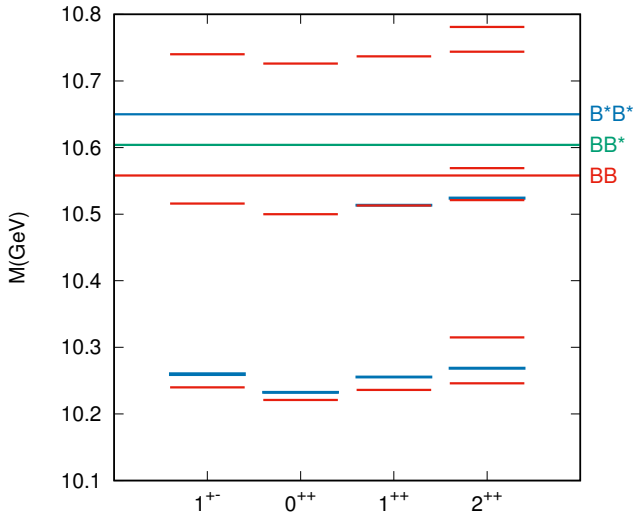


Figure 6. Bottomonium spectrum in the energy region of $2P$ and $3P$ states. Blue boxes show the states in the Particle Data Group [7]. The states in red are the pure $Q\bar{Q}$ states predicted by the model.

5.3. Threshold Cusps

These are enhancements of the cross sections near the opening of a threshold. One famous example is the measurement of the scattering lengths difference $a_0 - a_2$ in $\pi\pi$ scattering using a cusp-like enhancement in the $\pi^0\pi^0$ invariant mass distribution in the $K^\pm \to \pi^\pm\pi^0\pi^0$ decay [85]. It was first noticed in Ref. [86] and then proposed to be measured by Cabibbo [87]. Due to the very precise experimental data available, a very precise determination of this combination was performed [88] that was in very good agreement with χPT predictions.

This effect has been also used to explain strong energy dependencies near the threshold of invariant mass distributions, as in the case of Z_c and Z_b states [89,90]. The effect should be present when the interaction is attractive [91]; however, it has been argued [92] that such big effects may not appear without the existence of a nearby pole (bound, virtual, or resonance state).

One example of a threshold cusp effect in the hidden-charm sector is the $X(4140)$ resonance, a $J^{PC} = 1^{++}$ structure observed in the $\phi J/\psi$ invariant mass spectrum by many collaborations, such as CDF [93], D0 [94], CMS [95], Belle [96], BaBar [97], and LHCb [98]. Within the chiral quark model described above, a coupled calculation of the main open-charm channels [99] showed that the structure just above the $\phi J/\psi$ threshold is not caused by the effect of a nearby $c\bar{c}$ pole, but it is associated with the presence of the $D_s\bar{D}_s^*$ channel. The residual $D_s\bar{D}_s^*$ interaction is strong enough to show a rapid increase of the experimental counts, but too weak to develop a bound or virtual state.

Even more interesting is the case of Z_c and Z_b states. For the Zc(3900), there exist analyses of the BESIII data considering two-body coupled channels and triangle singularities [100–102]. In the chiral quark model, the Z_c states have been studied in Ref. [103]. The $Z_c(3900)^{\pm}/Z_c(3885)^{\pm}$ and $Z_c(4020)^{\pm}$ are meson states in the charmonium energy range. The fact that they are charged rules out the possibility of being $c\bar{c}$ states, and, at least, four quarks are needed. The nature of these charged states is still an open question.

The $Z_c(3900)$ was discovered by the BESIII [104] and Belle [105] Collaborations in the $\pi J/\psi$ invariant mass distribution of the reaction $e^+e^- \to \pi^+\pi^- J/\psi$. It was then seen by the BESIII Collaboration [106] in the $D\bar{D}^*$ invariant mass distribution of the $e^+e^- \to \pi^{\pm}(D\bar{D}^*)^{\mp}$ reaction with a lower mass and was referred to as the $Z_c(3885)$, although now it is seen as the same state. Soon after this discovery, the BESIII Collaboration reported the discovery of another charged state, the $Z_c(4020)$, in the reaction $e^+e^- \to \pi^+\pi^- h_c$ [107]. Later on, BESIII also reported about the neutral partner [108], completing the isospin triplet.

In Ref. [103], $D^*\bar{D}^{(*)}$ was analyzed in the sector $I^G(J^{PC}) = 1^+(1^{+-})$, within the formalism previously mentioned. Although here there is no $q\bar{q}$ state coupled to two-meson components, this system is interesting for another reason. There are two close-by channels that one would not expect to have an important effect, the $\pi J/\psi$ and $\rho\eta_c$, since the interactions between these mesons are expected to be small. However, the non-diagonal interaction $D^*\bar{D}^{(*)} - \pi J/\psi$ and $D^*\bar{D}^{(*)} - \rho\eta_c$ are dominant, and they do not generate bound states but virtual states.

In Table 5, we give the pole position for the states corresponding to the $Z_c(3900)^{\pm}$ and $Z_c(4020)^{\pm}$. The poles are below the $D\bar{D}^*$ and $D^*\bar{D}^*$ thresholds, respectively, and in the second Riemann sheet corresponding to virtual states. Despite these poles already emerging when the main open-charm channels are included, other channels are important in order to describe the experimental lineshapes. Lineshapes for different reactions are shown in Figures 7 and 8. Although we find poles on the S-matrix that produce structures in the lineshapes, in some cases, they don't seem enough, which supports the idea that a threshold cusp effect might not be sufficient to describe the experimental data without the existence of some associated pole.

Table 5. The S-matrix pole positions, in MeV/c^2, for different coupled-channels calculations [103]. The included channels for each case are shown in the first column. Poles are given in the second and fourth columns by the value of the complex energy in a specific Riemann sheet (RS). The RS columns indicate whether the pole has been found in the first (F) or second (S) Riemann sheet of a given channel. Each channel in the coupled-channels calculation is represented as an array's element, ordered with increasing energy.

Calculation	$Z_c(3900)$ Pole	RS	$Z_c(4020)$ Pole	RS
$D\bar{D}^*$	$3871.37 - 2.17\,i$	(S)	-	-
$D\bar{D}^* + D^*\bar{D}^*$	$3872.27 - 1.85\,i$	(S,F)	$4014.16 - 0.10\,i$	(S,S)
$\rho\eta_c + D\bar{D}^*$	$3871.32 - 0.00\,i$	(S,S)	-	-
$\rho\eta_c + D\bar{D}^* + D^*\bar{D}^*$	$3872.07 - 0.00\,i$	(S,S,F)	$4013.10 - 0.00\,i$	(S,S,S)
$\pi J/\psi + \rho\eta_c + D\bar{D}^* + D^*\bar{D}^*$	$3871.74 - 0.00\,i$	(S,S,S,F)	$4013.21 - 0.00\,i$	(S,S,S,S)

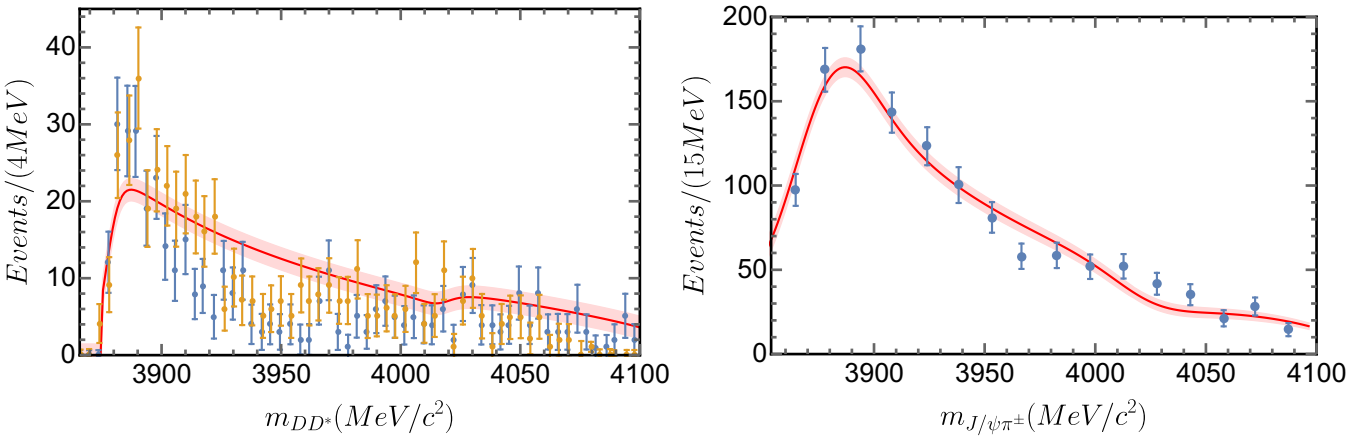


Figure 7. Line shapes for $D\bar{D}^*$ (left panel) and $\pi J/\psi$ (right panel) at $\sqrt{s} = 4.26$ GeV [103]. Experimental data are from Refs. [109,110], respectively. The theoretical line shapes have been convoluted with the experimental resolution. The line-shape's 68% uncertainty is shown as a shadowed area.

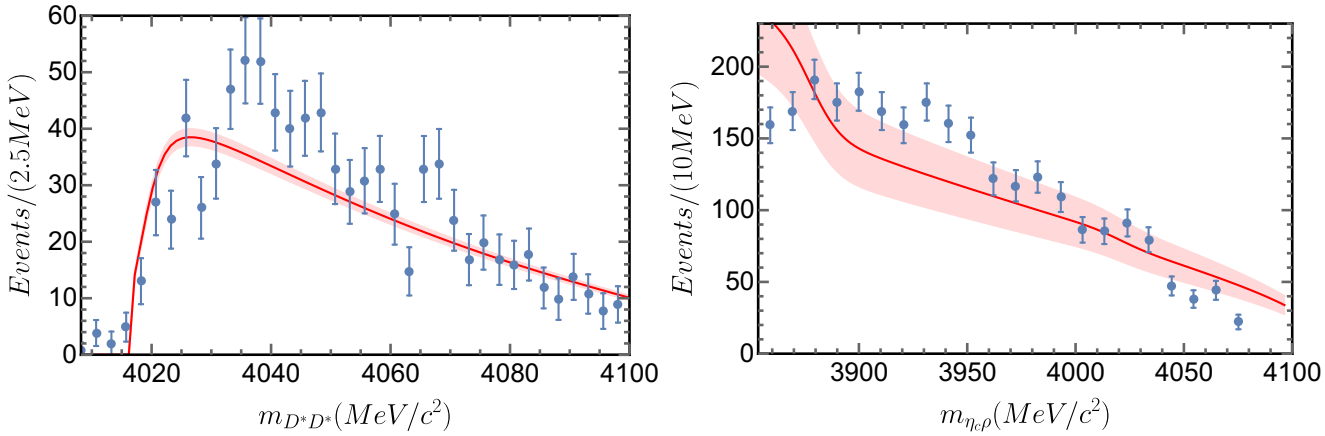


Figure 8. Line shapes for $D^*\bar{D}^*$ (left panel) and $\eta_c\rho$ (right panel) at $\sqrt{s} = 4.26$ GeV [103]. Experimental data for $D^*\bar{D}^*$ are from Ref. [111]. The theoretical line shapes have been convoluted with the experimental resolution. The line-shape's 68%-uncertainty is shown as a shadowed area.

6. Conclusions

The naive quark model has been very successful in describing heavy hadron phenomenology for a very long time. However, since 2003, it seems clear that the coupling with two hadron states are of relevance to describe the phenomenology of new discovered states.

In this work, we have described how a microscopic quark model can be used, and, in particular, the chiral quark model, to describe systems in which conventional quark model states can couple to two-hadron states in a consistent framework. Although these effects are of no relevance in many low-lying states, keeping the validity of the naive quark model, in some cases, the effects can be very important.

This framework has been used during the last few years to study the meson spectrum, and we have shown a few examples where deviations from naive quark model expectations are of special relevance. In fact, threshold effects can generate deviations from expected results predicted by well-known symmetries such as HFS or HQQS, highlighting the importance of analyzing such effects especially in the heavy meson and baryon sectors.

Author Contributions: Conceptualization and methodology, P.G.O. and D.R.E.; Software, P.G.O. and D.R.E.; Validation, P.G.O. and D.R.E.; Writing—original draft preparation, P.G.O. and D.R.E.; Writing—review and editing, P.G.O. and D.R.E.; Funding acquisition, P.G.O. and D.R.E.; All authors have read and agreed to the published version of the manuscript.

Funding: This work has been funded by the Ministerio de Economía, Industria y Competitividad under Contract No. FPA2016-77177-C2-2-P and Ministerio de Ciencia, Innovación y Universidades under Contract No. PID2019-105439GB-C22, and by the EU Horizon 2020 research and innovation program, STRONG-2020 project, under Grant No. 824093.

Institutional Review Board Statement: Not applicable.

Informed Consent Statement: Not applicable.

Data Availability Statement: Not applicable.

Conflicts of Interest: The authors declare no conflict of interest. The funders had no role in the design of the study; in the collection, analyses, or interpretation of data; in the writing of the manuscript, or in the decision to publish the results.

Abbreviations

The following abbreviations are used in this manuscript:

HQQS	Heavy Quark Spin Symmetry
HFS	Heavy Flavor Symmetry
χPT	Chiral Perturbation Theory
QCD	Quantum Chromodynamics

References

1. Aubert, J.J.; Becker, U.; Biggs, P.J.; Burger, J.; Chen, M.; Everhart, G.; Goldhagen, P.; Leong, J.; McCorriston, T.; Rhoades, T.G.; et al. Experimental Observation of a Heavy Particle *J*. *Phys. Rev. Lett.* **1974**, *33*, 1404–1406. [CrossRef]
2. Augustin, J.E.; Boyarski, A.M.; Breidenbach, M.; Bulos, F.; Dakin, J.T.; Feldman, G.J.; Fischer, G.E.; Fryberger, D.; Hanson, G.; Jean-Marie, B.; et al. Discovery of a Narrow Resonance in e^+e^- Annihilation. *Phys. Rev. Lett.* **1974**, *33*, 1406–1408. [CrossRef]
3. Glashow, S.L.; Iliopoulos, J.; Maiani, L. Weak Interactions with Lepton-Hadron Symmetry. *Phys. Rev. D* **1970**, *2*, 1285–1292. [CrossRef]
4. Herb, S.W.; Hom, D.C.; Lederman, L.M.; Sens, J.C.; Snyder, H.D.; Yoh, J.K.; Appel, J.A.; Brown, B.C.; Brown, C.N.; Innes, W.R.; et al. Observation of a Dimuon Resonance at 9.5 GeV in 400-GeV Proton-Nucleus Collisions. *Phys. Rev. Lett.* **1977**, *39*, 252–255. [CrossRef]
5. Kelly, R.L.; Horne, C.P.; Losty, M.J.; Rittenberg, A.; Shimada, T.; Trippe, T.G.; Wohl, C.G.; Yost, G.P.; Barash-Schmidt, N.; Bricman, C.; et al. Review of particle properties. *Rev. Mod. Phys.* **1980**, *52*, S1–S286. [CrossRef]
6. Hagiwara, K.; Montanet, L.; Barnett, R.M.; Groom, D.E.; Trippe, T.G.; Wohl, C.G.; Armstrong, B.; Wagman, G.S.; Murayama, H.; Stone, J.; et al. Review of Particle Properties. *Phys. Rev. D* **2002**, *66*, 010001. [CrossRef]
7. Particle Data Group; Zyla, P.A.; Barnett, R.M.; Beringer, J.; Dahl, O.; Dwyer, D.A.; Groom, D.E.; Lin, C.J.; Lugovsky, K.S.; Pianori, E.; et al. Review of Particle Physics. *Prog. Theor. Exp. Phys.* **2020**, *2020*, 083C01. [CrossRef]
8. Cazzoli, E.G.; Cnops, A.M.; Connolly, P.L.; Louttit, R.I.; Murtagh, M.J.; Palmer, R.B.; Samios, N.P.; Tso, T.T.; Williams, H.H. Evidence for $\Delta S = -\Delta Q$ Currents or Charmed-Baryon Production by Neutrinos. *Phys. Rev. Lett.* **1975**, *34*, 1125–1128. [CrossRef]
9. Eichten, E.; Gottfried, K.; Kinoshita, T.; Lane, K.D.; Yan, T.M. Charmonium: The Model. *Phys. Rev. D* **1978**, *17*, 3090–3117; Erratum in **1980**, *21*, 313. [CrossRef]
10. Eichten, E.; Gottfried, K.; Kinoshita, T.; Lane, K.D.; Yan, T.M. Charmonium: Comparison with Experiment. *Phys. Rev. D* **1980**, *21*, 203–233. [CrossRef]
11. Gupta, S.N.; Radford, S.F.; Repko, W.W. Semirelativistic Potential Model for Charmonium. *Phys. Rev. D* **1985**, *31*, 160. [CrossRef] [PubMed]
12. Barnes, T.; Close, F.E.; Page, P.R.; Swanson, E.S. Higher quarkonia. *Phys. Rev. D* **1997**, *55*, 4157–4188. [CrossRef]
13. Ebert, D.; Faustov, R.N.; Galkin, V.O. Properties of heavy quarkonia and B_c mesons in the relativistic quark model. *Phys. Rev. D* **2003**, *67*, 014027. [CrossRef]
14. Eichten, E.; Godfrey, S.; Mahlke, H.; Rosner, J.L. Quarkonia and their transitions. *Rev. Mod. Phys.* **2008**, *80*, 1161–1193. [CrossRef]
15. Danilkin, I.V.; Simonov, Y.A. Channel coupling in heavy quarkonia: Energy levels, mixing, widths and new states. *Phys. Rev. D* **2010**, *81*, 074027. [CrossRef]
16. Ferretti, J.; Santopinto, E. Higher mass bottomonia. *Phys. Rev. D* **2014**, *90*, 094022. [CrossRef]
17. Godfrey, S.; Moats, K. Bottomonium Mesons and Strategies for their Observation. *Phys. Rev. D* **2015**, *92*, 054034. [CrossRef]
18. Caswell, W.E.; Lepage, G.P. Effective Lagrangians for Bound State Problems in QED, QCD, and Other Field Theories. *Phys. Lett. B* **1986**, *167*, 437–442. [CrossRef]
19. Pineda, A.; Soto, J. Effective field theory for ultrasoft momenta in NRQCD and NRQED. *Nucl. Phys. B Proc. Suppl.* **1998**, *64*, 428–432. [CrossRef]

20. Brambilla, N.; Pineda, A.; Soto, J.; Vairo, A. Effective Field Theories for Heavy Quarkonium. *Rev. Mod. Phys.* **2005**, *77*, 1423. [CrossRef]
21. Dudek, J.J.; Edwards, R.G.; Mathur, N.; Richards, D.G. Charmonium excited state spectrum in lattice QCD. *Phys. Rev. D* **2008**, *77*, 034501. [CrossRef]
22. Gray, A.; Allison, I.; Davies, C.T.H.; Dalgic, E.; Lepage, G.P.; Shigemitsu, J.; Wingate, M. The Upsilon spectrum and m(b) from full lattice QCD. *Phys. Rev. D* **2005**, *72*, 094507. [CrossRef]
23. Meinel, S. The Bottomonium spectrum from lattice QCD with 2+1 flavors of domain wall fermions. *Phys. Rev. D* **2009**, *79*, 094501. [CrossRef]
24. Gottfried, K. The spectroscopy of massive quark-antiquark systems, Progress in Particle and Nuclear Physics. *Prog. Part. Nucl. Phys.* **1982**, *8*, 49–71. [CrossRef]
25. Gostev, V.B.; Mineev, V.S.; Frenkin, A.R. The inverse problem of quantum mechanics for a linear potentia. *Theor. Math. Phys.* **1983**, *56*, 682–686. [CrossRef]
26. Sumino, Y. QCD potential as a "Coulomb-plus-linear" potential. *Phys. Lett. B* **2003**, *571*, 173–183. [CrossRef]
27. Mateu, V.; Ortega, P.G.; Entem, D.R.; Fernández, F. Calibrating the Naïve Cornell Model with NRQCD. *Eur. Phys. J. C* **2019**, *79*, 323. [CrossRef]
28. Copley, L.A.; Isgur, N.; Karl, G. Charmed baryons in a quark model with hyperfine interactions. *Phys. Rev. D* **1979**, *20*, 768–775. [CrossRef]
29. Stanley, D.P.; Robsen, D. Do Quarks Interact Pairwise and Satisfy the Color Hypothesis? *Phys. Rev. Lett.* **1980**, *45*, 235–238. [CrossRef]
30. Choi, S.K.; Olsen, S.L.; Abe, K.; Abe, T.; Adachi, I.; Ahn, B.S.; Aihara, H.; Akai, K.; Akatsu, M.; Akemoto, M.; et al. Observation of a Narrow Charmoniumlike State in Exclusive $B^{\pm} \to K^{\pm}\pi^{+}\pi^{-}J/\psi$ Decays. *Phys. Rev. Lett.* **2003**, *91*, 262001. [CrossRef] [PubMed]
31. Acosta, D.; Affolder, T.; Ahn, M.H.; Akimoto, T.; Albrow, M.G.; Ambrose, D.; Amerio, S.; Amidei, D.; Anastassov, A.; Anikeev, K.; et al. Observation of the Narrow State $X(3872) \to J/\psi\pi^{+}\pi^{-}$ in $\overline{p}p$ Collisions at $\sqrt{s} = 1.96$ TeV. *Phys. Rev. Lett.* **2004**, *93*, 072001. [CrossRef]
32. Abazov, V.M.; Abbott, B.; Abolins, M.; Acharya, B.S.; Adams, D.L.; Adams, M.; Adams, T.; Agelou, M.; Agram, J.L.; Ahmed, S.N.; et al. Observation and Properties of the $X(3872)$ Decaying to $J/\psi\pi^{+}\pi^{-}$ in $p\overline{p}$ Collisions at $\sqrt{s} = 1.96$ TeV. *Phys. Rev. Lett.* **2004**, *93*, 162002. [CrossRef]
33. Aubert, B.; Barate, R.; Boutigny, D.; Couderc, F.; Gaillard, J.M.; Hicheur, A.; Karyotakis, Y.; Lees, J.P.; Tisserand, V.; Zghiche, A.; et al. Study of the $B^{-} \to J/\psi K^{-}\pi^{+}\pi^{-}$ decay and measurement of the $B^{-} \to X(3872)K^{-}$ branching fraction. *Phys. Rev. D* **2005**, *71*, 071103. [CrossRef]
34. Aaij, R.; Adeva, B.; Adinolfi, M.; Affolder, A.; Ajaltouni, Z.; Akar, S.; Albrecht, J.; Alessio, F.; Alexander, M.; Ali, S.; et al. Observation of $J/\psi p$ Resonances Consistent with Pentaquark States in $\Lambda_b^0 \to J/\psi K^{-} p$ Decays. *Phys. Rev. Lett.* **2015**, *115*, 072001. [CrossRef]
35. Aaij, R.; Beteta, C.A.; Adeva, B.; Adinolfi, M.; Aidala, C.A.; Ajaltouni, Z.; Akar, S.; Albicocco, P.; Albrecht, J.; Alessio, F.; et al. Observation of a Narrow Pentaquark State, $P_c(4312)^{+}$, and of the Two-Peak Structure of the $P_c(4450)^{+}$. *Phys. Rev. Lett.* **2019**, *122*, 222001. [CrossRef] [PubMed]
36. Manohar, A.; Georgi, H. Chiral quarks and the non-relativistic quark model. *Nucl. Phys. B* **1984**, *234*, 189–212. [CrossRef]
37. Fernandez, F.; Valcarce, A.; Straub, U.; Faessler, A. The nucleon-nucleon interaction in terms of quark degrees of freedom. *J. Phys. G Nucl. Part. Phys.* **1993**, *19*, 2013–2026. [CrossRef]
38. Vijande, J.; Fernández, F.; Valcarce, A. Constituent quark model study of the meson spectra. *J. Phys. G Nucl. Part. Phys.* **2005**, *31*, 481–506. [CrossRef]
39. Burgio, G.; Schröck, M.; Reinhardt, H.; Quandt, M. Running mass, effective energy, and confinement: The lattice quark propagator in Coulomb gauge. *Phys. Rev. D* **2012**, *86*, 014506. [CrossRef]
40. Bali, G.S. QCD forces and heavy quark bound states. *Phys. Rep.* **2001**, *343*, 1–136. [CrossRef]
41. Bali, G.S.; Neff, H.; Düssel, T.; Lippert, T.; Schilling, K. Observation of string breaking in QCD. *Phys. Rev. D* **2005**, *71*, 114513. [CrossRef]
42. De Rújula, A.; Georgi, H.; Glashow, S.L. Hadron masses in a gauge theory. *Phys. Rev. D* **1975**, *12*, 147–162. [CrossRef]
43. Segovia, J.; Yasser, A.M.; Entem, D.R.; Fernández, F. $J^{PC} = 1^{--}$ hidden charm resonances. *Phys. Rev. D* **2008**, *78*, 114033. [CrossRef]
44. Segovia, J.; Entem, D.R.; Fernandez, F.; Hernandez, E. Constituent quark model description of charmonium phenomenology. *Int. J. Mod. Phys. E* **2013**, *22*, 1330026. [CrossRef]
45. Kamimura, M. Nonadiabatic coupled-rearrangement-channel approach to muonic molecules. *Phys. Rev. A* **1988**, *38*, 621–624. [CrossRef] [PubMed]
46. Hiyama, E.; Kino, Y.; Kamimura, M. Gaussian expansion method for few-body systems. *Prog. Part. Nucl. Phys.* **2003**, *51*, 223–307. [CrossRef]
47. Hiyama, E. Gaussian expansion method for few-body systems and its applications to atomic and nuclear physics. *Prog. Theor. Exp. Phys.* **2012**, *2012*, 01A204. [CrossRef]

48. Morton, D.; Wu, Q.; Drake, G.W. Energy Levels for the Stable Isotopes of Atomic Helium (4He I and 3He I). *Can. J. Phys.* **2006**, *84*, 83–105. [CrossRef]
49. Bhaduri, R.K.; Cohler, L.E.; Nogami, Y. A unified potential for mesons and baryons. *Il Nuovo Cimento A* **1981**, *65*. [CrossRef]
50. Silvestre-Brac, B. Spectrum and Static Properties of Heavy Baryons. *Few-Body Syst.* **1996**, *20*. [CrossRef]
51. Kandula, D.Z.; Gohle, C.; Pinkert, T.J.; Ubachs, W.; Eikema, K.S.E. Extreme Ultraviolet Frequency Comb Metrology. *Phys. Rev. Lett.* **2010**, *105*, 063001. [CrossRef] [PubMed]
52. Martin, W.C. Energy Levels of Neutral Helium (4He I). *J. Phys. Chem. Ref. Data* **1973**, *2*, 257–266. [CrossRef]
53. Tech, J.L.; Ward, J.F. Accurate Wavelength Measurement of the $1s2p\,^3P^0 - 2p^2\,^3P$ Transition in ^{4}He I. *Phys. Rev. Lett.* **1971**, *27*, 367–370. [CrossRef]
54. Micu, L. Decay rates of meson resonances in a quark model. *Nucl. Phys.* **1969**, *B10*, 521–526. [CrossRef]
55. Le Yaouanc, A.; Oliver, L.; Pène, O.; Raynal, J.C. "Naive" Quark-Pair-Creation Model of Strong-Interaction Vertices. *Phys. Rev. D* **1973**, *8*, 2223–2234. [CrossRef]
56. Le Yaouanc, A.; Oliver, L.; Pène, O.; Raynal, J.C. Naive quark-pair—Creation model and baryon decays. *Phys. Rev. D* **1974**, *9*, 1415–1419. [CrossRef]
57. Yaouanc, A.L.; Oliver, L.; Pene, O.; Raynal, J.C. Strong decays of $\psi(4028)$ as a radial excitation of charmonium. *Phys. Lett. B* **1977**, *71*, 397–399. [CrossRef]
58. Yaouanc, A.L.; Oliver, L.; Pène, O.; Raynal, J. Why is $\psi(4414)$ so narrow? *Phys. Lett. B* **1977**, *72*, 57–61. [CrossRef]
59. Ackleh, E.S.; Barnes, T.; Swanson, E.S. On the mechanism of open-flavor strong decays. *Phys. Rev. D* **1996**, *54*, 6811–6829. [CrossRef]
60. Segovia, J.; Entem, D.; Fernández, F. Scaling of the P03 strength in heavy meson strong decays. *Phys. Lett. B* **2012**, *715*, 322–327. [CrossRef]
61. Bijker, R.; Santopinto, E. Unquenched quark model for baryons: Magnetic moments, spins, and orbital angular momenta. *Phys. Rev. C* **2009**, *80*, 065210. [CrossRef]
62. Heikkilä, K.; Törnqvist, N.A.; Ono, S. Heavy $c\bar{c}$ and $b\bar{b}$ quarkonium states and unitarity effects. *Phys. Rev. D* **1984**, *29*, 110–120. [CrossRef]
63. Baru, V.; Hanhart, C.; Kalashnikova, Y.S.; Kudryavtsev, A.E.; Nefediev, A.V. Interplay of quark and meson degrees of freedom in a near-threshold resonance. *Eur. Phys. J A* **2010**, *44*, 93. [CrossRef]
64. Ortega, P.G.; Entem, D.R.; Fernández, F. Unquenching the Quark Model in a Nonperturbative Scheme. *Adv. High Energy Phys.* **2019**, *2019*, 3465159. [CrossRef]
65. Abulencia, A.; Acosta, D.; Adelman, J.; Affolder, T.; Akimoto, T.; Albrow, M.G.; Ambrose, D.; Amerio, S.; Amidei, D.; Anastassov, A.; et al. Measurement of the Dipion Mass Spectrum in $X(3872) \to J/\psi\pi^+\pi^-$ Decays. *Phys. Rev. Lett.* **2006**, *96*, 102002. [CrossRef] [PubMed]
66. Abe, K. Evidence for X(3872) —> γ J / ψ and the sub-threshold decay X(3872) —> ω J / ψ. Lepton and photon interactions at high energies. In Proceedings of the 22nd International Symposium, LP 2005, Uppsala, Sweden, 30 June–5 July 2005.
67. Aushev, T.; Eidelman, S.; Gabyshev, N.; Shwartz, B.; Usov, Y.; Zhulanov, V.; Zyukova, O.; Drutskoy, A.; Goldenzweig, P.; Lange, J.S.; et al. Study of the $B \to X(3872)(\to D^{*0}\overline{D}^0)K$ decay. *Phys. Rev. D* **2010**, *81*, 031103. [CrossRef]
68. Guo, F.K. Novel Method for Precisely Measuring the $X(3872)$ Mass. *Phys. Rev. Lett.* **2019**, *122*, 202002. [CrossRef]
69. Aaij, R.; Abellan Beteta, C.; Ackernley, T.; Adeva, B.; Adinolfi, M.; Afsharnia, H.; Aidala, C.A.; Aiola, S.; Ajaltouni, Z.; Akar, S.; et al. Study of the $\psi_2(3823)$ and $\chi_{c1}(3872)$ states in $B^+ \to (J\psi\pi^+\pi^-)K^+$ decays. *J. High Energy Phys.* **2020**, *08*, 123. [CrossRef]
70. Swanson, E.S. Diagnostic decays of the X(3872). *Phys. Lett. B* **2004**, *598*, 197–202. [CrossRef]
71. Gamermann, D.; Oset, E. Isospin breaking effects in the $X(3872)$ resonance. *Phys. Rev. D* **2009**, *80*, 014003. [CrossRef]
72. Gamermann, D.; Nieves, J.; Oset, E.; Arriola, E.R. Couplings in coupled channels versus wave functions: Application to the $X(3872)$ resonance. *Phys. Rev. D* **2010**, *81*, 014029. [CrossRef]
73. Ortega, P.G.; Segovia, J.; Entem, D.R.; Fernández, F. Coupled channel approach to the structure of the $X(3872)$. *Phys. Rev. D* **2010**, *81*, 054023. [CrossRef]
74. Ferretti, J.; Galatà, G.; Santopinto, E. Interpretation of the $X(3872)$ as a charmonium state plus an extra component due to the coupling to the meson-meson continuum. *Phys. Rev. C* **2013**, *88*, 015207. [CrossRef]
75. Ortega, P.G.; Entem, D.R.; Fernández, F. Molecular structures in the charmonium spectrum: theXYZpuzzle. *J. Phys. G Nucl. Part. Phys.* **2013**, *40*, 065107. [CrossRef]
76. Burns, T.J. Phenomenology of Pc(4380)+, Pc(4450)+ and related states. *Eur. Phys. J. A* **2015**, *51*, 152. [CrossRef]
77. Guo, F.K.; Jing, H.J.; Meißner, U.G.; Sakai, S. Isospin breaking decays as a diagnosis of the hadronic molecular structure of the $P_c(4457)$. *Phys. Rev. D* **2019**, *99*, 091501. [CrossRef]
78. Nieves, J.; Pavón Valderrama, M. Heavy quark spin symmetry partners of the $X(3872)$. *Phys. Rev. D* **2012**, *86*, 056004. [CrossRef]
79. Hidalgo-Duque, C.; Nieves, J.; Valderrama, M.P. Light flavor and heavy quark spin symmetry in heavy meson molecules. *Phys. Rev. D* **2013**, *87*, 076006. [CrossRef]
80. Baru, V.; Epelbaum, E.; Filin, A.A.; Hanhart, C.; Nefediev, A.V. Molecular partners of the X(3872) from heavy-quark spin symmetry: a fresh look. *EPJ Web Conf.* **2017**, *137*, 06002. [CrossRef]
81. Guo, F.K.; Hidalgo-Duque, C.; Nieves, J.; Pavón Valderrama, M. Consequences of heavy-quark symmetries for hadronic molecules. *Phys. Rev. D* **2013**, *88*, 054007. [CrossRef]

82. Entem, D.R.; Ortega, P.G.; Fernández, F. Partners of the X(3872) and heavy quark spin symmetry breaking. *AIP Conf. Proc.* **2016**, *1735*, 060006. [CrossRef]
83. Cincioglu, E.; Nieves, J.; Ozpineci, A.; Yilmazer, A.U. Quarkonium Contribution to Meson Molecules. *Eur. Phys. J. C* **2016**, *76*, 576. [CrossRef]
84. Ortega, P.G.; Segovia, J.; Entem, D.R.; Fernández, F. Charmonium resonances in the 3.9 GeV/c2 energy region and the X(3915)/X(3930) puzzle. *Phys. Lett. B* **2018**, *778*, 1–5. [CrossRef]
85. Batley, J.; Lazzeroni, C.; Munday, D.J.; Slater, M.W.; Wotton, S.A.; Arcidiacono, R.; Bocquet, G.; Cabibbo, N.; Ceccucci, A.; Cundy, D.; et al. Observation of a cusp-like structure in the $\pi^0\pi^0$ invariant mass distribution from $K^\pm \to \pi^\pm\pi^0\pi^0$ decay and determination of the $\pi\pi$ scattering lengths. *Phys. Lett. B* **2006**, *633*, 173–182. [CrossRef]
86. Budini, P.; Fonda, L. Pion-Pion Interaction from Threshold Anomalies in K^+ Decay. *Phys. Rev. Lett.* **1961**, *6*, 419–421. [CrossRef]
87. Cabibbo, N. Determination of the $a_0 - a_2$ Pion Scattering Length from $K^+ \to \pi^+\pi^0\pi^0$ Decay. *Phys. Rev. Lett.* **2004**, *93*, 121801. [CrossRef]
88. Cabibbo, N.; Isidori, G. Pion-pion scattering and the K→3π decay amplitudes. *J. High Energy Phys.* **2005**, *2005*, 021. [CrossRef]
89. Bugg, D.V. An explanation of Belle states Z b (10610) and Z b (10650). *EPL (Europhys. Lett.)* **2011**, *96*, 11002. [CrossRef]
90. Swanson, E.S. Z_b and Z_c exotic states as coupled channel cusps. *Phys. Rev. D* **2015**, *91*, 034009. [CrossRef]
91. Dong, X.K.; Guo, F.K.; Zou, B.S. Why there are many threshold structures in hadron spectrum with heavy quarks. *arXiv* **2020**, arXiv:2011.14517.
92. Guo, F.K.; Hanhart, C.; Wang, Q.; Zhao, Q. Could the near-threshold XYZ states be simply kinematic effects? *Phys. Rev. D* **2015**, *91*, 051504. [CrossRef]
93. Aaltonen, T. Observation of the $Y(4140)$ structure in the $J/\psi\phi$ Mass Spectrum in $B^\pm \to J/\psi\phi K$ decays. *arXiv* **2011**, arXiv:1101.6058.
94. Abazov, V.M. Inclusive Production of the X(4140) State in $p\overline{p}$ Collisions at D0. *Phys. Rev. Lett.* **2015**, *115*, 232001. [CrossRef] [PubMed]
95. Chatrchyan, S. Observation of a peaking structure in the $J/\psi\phi$ mass spectrum from $B^\pm \to J/\psi\phi K^\pm$ decays. *Phys. Lett.* **2014**, *B734*, 261–281. [CrossRef]
96. Shen, C.P.; Yuan, C.Z.; Aihara, H.; Arinstein, K.; Aushev, T.; Bakich, A.M.; Balagura, V.; Barberio, E.; Bay, A.; Belous, K.; et al. Evidence for a new resonance and search for the Y(4140) in the gamma gamma —> phi J/psi process. *Phys. Rev. Lett.* **2010**, *104*, 112004. [CrossRef] [PubMed]
97. Lees, J.P. Study of $B^{\pm,0} \to J/\psi K^+K^-K^{\pm,0}$ and search for $B^0 \to J/\psi\phi$ at BABAR. *Phys. Rev.* **2015**, *D91*, 012003. [CrossRef]
98. Aaij, R. Observation of $J/\psi\phi$ structures consistent with exotic states from amplitude analysis of $B^+ \to J/\psi\phi K^+$ decays. *arXiv* **2016**, arXiv:1606.07895.
99. Ortega, P.G.; Segovia, J.; Entem, D.R.; Fernández, F. Canonical description of the new LHCb resonances. *Phys. Rev. D* **2016**, *94*, 114018. [CrossRef]
100. Albaladejo, M.; Guo, F.K.; Hidalgo-Duque, C.; Nieves, J. Zc(3900): What has been really seen? *Phys. Lett. B* **2016**, *755*, 337–342. [CrossRef]
101. Pilloni, A.; Fernández-Ramírez, C.; Jackura, A.; Mathieu, V.; Mikhasenko, M.; Nys, J.; Szczepaniak, A. Amplitude analysis and the nature of the Zc(3900). *Phys. Lett. B* **2017**, *772*, 200–209. [CrossRef]
102. Ikeda, Y.; Aoki, S.; Doi, T.; Gongyo, S.; Hatsuda, T.; Inoue, T.; Iritani, T.; Ishii, N.; Murano, K.; Sasaki, K. Fate of the Tetraquark Candidate $Z_c(3900)$ from Lattice QCD. *Phys. Rev. Lett.* **2016**, *117*, 242001. [CrossRef] [PubMed]
103. Ortega, P.G.; Segovia, J.; Entem, D.R.; Fernández, F. The Z_c structures in a coupled-channels model. *Eur. Phys. J. C* **2019**, *79*, 78. [CrossRef]
104. Ablikim, M.; Achasov, M.N.; Albayrak, O.; Ambrose, D.J.; An, F.F.; An, Q.; Bai, J.Z.; Ferroli, R.B.; Ban, Y.; Becker, J.; et al. Observation of a Charged Charmoniumlike Structure in $e^+e^- \to \pi^+\pi^- J/\psi$ at $\sqrt{s}$=4.26 GeV. *Phys. Rev. Lett.* **2013**, *110*, 252001. [CrossRef]
105. Liu, Z.Q.; Shen, C.P.; Yuan, C.Z.; Adachi, I.; Aihara, H.; Asner, D.M.; Aulchenko, V.; Aushev, T.; Aziz, T.; Bakich, A.M.; et al. Study of $e^+e^- \to \pi^+\pi^- J/\psi$ and Observation of a Charged Charmoniumlike State at Belle. *Phys. Rev. Lett.* **2013**, *110*, 252002. [CrossRef] [PubMed]
106. Ablikim, M.; Achasov, M.N.; Albayrak, O.; Ambrose, D.J.; An, F.F.; An, Q.; Bai, J.Z.; Baldini Ferroli, R.; Ban, Y.; Becker, J.; et al. Observation of a Charged $(D\overline{D}^*)^\pm$ Mass Peak in $e^+e^- \to \pi D\overline{D}^*$ at $\sqrt{s} = 4.26$ GeV. *Phys. Rev. Lett.* **2014**, *112*, 022001. [CrossRef] [PubMed]
107. Ablikim, M.; Achasov, M.N.; Albayrak, O.; Ambrose, D.J.; An, F.F.; An, Q.; Bai, J.Z.; Baldini Ferroli, R.; Ban, Y.; Becker, J.; et al. Observation of a Charged Charmoniumlike Structure $Z_c(4020)$ and Search for the $Z_c(3900)$ in $e^+e^- \to \pi^+\pi^- h_c$. *Phys. Rev. Lett.* **2013**, *111*, 242001. [CrossRef] [PubMed]
108. Ablikim, M.; Achasov, M.N.; Ai, X.C.; Albayrak, O.; Albrecht, M.; Ambrose, D.J.; Amoroso, A.; Lou, X.; BESIII Collaboration. Observation of $e^+e^- \to \pi^0\pi^0 h_c$ and a Neutral Charmoniumlike Structure $Z_c(4020)^0$. *Phys. Rev. Lett.* **2014**, *113*, 212002. [CrossRef]
109. Ablikim, M.; Achasov, M.N.; Ai, X.C.; Albayrak, O.; Albrecht, M.G.; Ambrose, D.J.; BESIII Collaboration. Confirmation of a charged charmoniumlike state $Z_c(3885)^\mp$ in $e^+e^- \to \pi^\pm(D\bar{D}^*)^\mp$ with double D tag. *Phys. Rev.* **2015**, *D92*, 092006. [CrossRef]

110. Ablikim, M.; Achasov, M.N.; Ai, X.C.; Albayrak, O.; Albrecht, M.; Ambrose, D.J.; Amoroso, A.; An, F.F.; An, Q.; Bai, J.Z.; et al. Determination of the Spin and Parity of the $Z_c(3900)$. *Phys. Rev. Lett.* **2017**, *119*, 072001. [CrossRef] [PubMed]
111. Ablikim, M.; Achasov, M.N.; Albayrak, O.; Ambrose, D.J.; An, F.F.; An, Q.; Bai, J.Z.; Ferroli, R.B.; Ban, Y.; Becker, J.; et al. Observation of a charged charmoniumlike structure in $e^+e^- \to (D^*\bar{D}^*)^\pm\pi^\mp$ at $\sqrt{s} = 4.26$ GeV. *Phys. Rev. Lett.* **2014**, *112*, 132001. [CrossRef] [PubMed]